

# 1 Environmentally Benign Fast-degrading Conductive 2 Composites

3 *Angelique F. Greene\*<sup>‡</sup>, Robert Abbel<sup>‡</sup>, Alankar A. Vaidya, Queenie Tanjay, Yi Chen, Regis Risani,*  
4 *Taryn Saggese, Maxime Barbier, Miruna Petcu, Mark West, Beatrix Theobald, Eva Gaugler and*  
5 *Kate Parker. <sup>‡</sup>Authors contributed equal work*

6 *Te Papa Tipu Innovation Park, Tītokorangi Drive, Rotorua, New Zealand 3010*

## 7 KEYWORDS

8 Enzyme, thermoplastic, conductive materials, plastic degradation, sensing, & biotechnology

9

## 10 ABSTRACT

11 An environmentally benign conductive composite that rapidly degrades in the presence of warm  
12 water via enzyme-mediated hydrolysis is described. This represents the first time that hydrolytic  
13 enzymes have been immobilized onto eco-friendly conductive carbon sources with the express  
14 purpose of degrading the encapsulating biodegradable plastic. Amano Lipase (AL) functionalized  
15 carbon nanofibers (CNF) were compounded with polycaprolactone (PCL) to produce the  
16 composite film CNF<sub>AL</sub>-PCL (thickness = ~600 μm; CNF<sub>AL</sub> = 20.0 wt.%). To serve as controls,  
17 films of the same thickness were also produced, including CNF-AL<sub>5</sub>-PCL (CNF mixed with AL  
18 & PCL; CNF = 19.2 wt.% & AL = 5.00 wt.%), CNF-PCL (CNF = 19.2 wt.%), AL<sub>x</sub>-PCL (AL = x  
19 = 1.00 or 5.00 wt.%), and PCL. The electrical performance of the CNF-containing composites was

20 measured, and conductivities of  $14.0 \pm 2$ ,  $22.0 \pm 5$ , and  $31.0 \pm 6$  (S/m) were observed for CNF<sub>AL</sub>-  
21 PCL, CNF-AL<sub>5</sub>-PCL, and CNF-PCL, respectively. CNF<sub>AL</sub>-PCL and control films were degraded  
22 in phosphate buffer (2.00 mg/mL film/buffer) at 50 °C and their average percent weight loss  
23 (Wt.<sub>avg</sub>%) was recorded over time. After three hours CNF<sub>AL</sub>-PCL degraded to a Wt.<sub>avg</sub>% of 90.0%  
24 and had completely degraded after eight hours. This was considerably faster than CNF-AL<sub>5</sub>-PCL,  
25 which achieved a total Wt.<sub>avg</sub>% of 34.0% after 16 days, and CNF-PCL which was with a Wt.<sub>avg</sub>% of  
26 7.00% after 16 days. Scanning electron microscopy experiments (SEM) found that CNF<sub>AL</sub>-PCL  
27 has more open pores on its surface and that it fractures faster during degradation experiments  
28 which exposes interior enzyme to water. An electrode made from CNF<sub>AL</sub>-PCL was fabricated and  
29 attached to an AL<sub>5</sub>-PCL support to form a fast-degrading thermal sensor. Resistance was measured  
30 over five cycles where the temperature was varied between 15.0 °C and 50.0 °C. The sensor was  
31 then degraded fully in buffer at 50 °C over a 48-hour period.

## 32 INTRODUCTION

33 Recently, the concept of enzyme-mediated plastic degradation has received substantial attention  
34 from the scientific community<sup>1-3</sup> and the popular press<sup>4-6</sup> due to the development of a thermally  
35 stable polyethylene terephthalate degrading enzyme (PETase)<sup>7</sup> which is more colloquially referred  
36 to as a “plastic eating enzyme.”<sup>5-8</sup> Such enzymes generally fall into the “hydrolase” family  
37 (esterases, lipases, proteases, aminases, etc.) meaning that they typically mediate a hydrolysis  
38 reaction in the backbone of the plastic via a catalytic triad/oxyanion hole motif at the active site.<sup>9</sup>  
39 For polyester plastics with readily hydrolyzable backbones such as polycaprolactone (PCL),  
40 polylactic acid (PLA), and polyhydroxybutyrate (PHB), enzymes such as common lipases,  
41 proteinase K, cutinases, and PHB depolymerase can facilitate degradation.<sup>10,11</sup> Delivery of the  
42 enzyme to the plastic can occur either externally or internally. External delivery methods usually

43 dissolve the enzyme in buffer which is placed in direct contact with the submerged plastic  
44 substrate.<sup>10,12,13</sup> Internal delivery methods generally refer to when the enzyme (immobilized or  
45 free) is physically embedded into the plastic which is then degraded from the inside out when  
46 water/buffer activates the enzyme via diffusion into the matrix.<sup>14-17</sup> Enzymatic plastics recycling,  
47 which focusses on plastic end-of-life, utilizes external delivery methods to facilitate breaking down  
48 large amounts of plastic waste to produce monomers that can either be repolymerized or be  
49 converted into other specialty chemicals for future use.<sup>18</sup> Internal delivery methods have been  
50 mostly found in the literature as a method to speed up the plastics degradation process with regards  
51 to compostable packaging.<sup>19,20</sup> However, there have not been many examples of this method being  
52 used to improve the end-of-life for plastics used in other more high-value applications, e.g.,  
53 electronics, which means that there is still an opportunity to explore this technology further.

54 Sensing and other electronic monitoring devices are ubiquitous in our everyday life and are  
55 especially important in industry where these instruments can be used to measure the freshness of  
56 produce in transit, environmental fluctuations, in agriculture, and numerous other applications.  
57 Most of these devices contain metals (e.g. silver; copper) and fossil-based materials (e.g. printed  
58 circuit board) , meaning that the end-of-life and toxicity of these devices can become an issue.<sup>21-</sup>  
59 <sup>23</sup> To solve this problem green or sustainable electronics are being developed to ameliorate these  
60 environmental issues.<sup>24</sup> Typical strategies include the substitution of metal-based conductive  
61 inks/materials with sustainably sourced carbon-based conductive materials, such as graphene or  
62 carbon nanomaterials, and replacing the body of the device/substrate with biodegradable polymers  
63 or natural materials to reduce its impact on the environment.<sup>25-27</sup> Recently, Beniwal et al. have  
64 showed that graphene-based carbon ink could be screen-printed onto a paper substrate to construct  
65 a humidity sensor with wireless communication.<sup>28</sup> Additionally, Tu et. al. have showed that

66 carbon-based inks could be printed onto dissolvable PVA/gelatin substrates for point of care  
67 testing.<sup>29</sup> Although these examples show advancement in green and biodegradable sensors, many  
68 applications require materials that are tear-proof, do not bio-foul quickly, but are guaranteed to  
69 degrade completely at the end of their service life. Biodegradable and compostable plastics are  
70 well-suited to tackle this problem, however, biodegradable plastics can suffer from slow or  
71 unreliable degradation.<sup>30,31</sup> Embedding hydrolytic enzymes into these biodegradable plastics  
72 would expedite the natural degradation process of these devices and provide a solution for this  
73 problem. Recently, Kwon et. al. showed that silver inks compounded with PCL could be printed  
74 onto the surface of a PCL substrate embedded with lipase to produce sensors that degrade rapidly  
75 in the presence of warm water allowing for the recovery and recycling of the silver ink.<sup>32</sup> Although  
76 this is a great stride forward for this technology, there are currently no systems that combine the  
77 fast-degrading properties of enzyme embedded compostable plastics with environmentally benign  
78 conductive carbon-based materials. .

79 Here, we demonstrate the development of a fast-degrading carbon-based conductive composite  
80 made from polycaprolactone and carbon nanofiber with immobilized lipase that rapidly breaks  
81 down in the presence of warm water. Carbon nanofibers (CNF) were chosen as an immobilization  
82 support and conductor due to their lower relative eco-toxicity compared to metal-based conductors  
83 and their potential to be manufactured from renewable/biobased resources (e.g., lignin).<sup>25,33</sup>  
84 Polycaprolactone (PCL) and Amano lipase (AL) were selected due to polycaprolactone's  
85 biodegradability and compostability and Amano Lipase's thermal stability.<sup>15</sup> This represents the  
86 first time that hydrolytic enzymes have been immobilized onto environmentally benign carbon  
87 nanomaterials to form an all-in-one conductive biocatalyst with the express goal of degrading an  
88 encapsulating biodegradable plastic. Additionally, as proof-of-concept this novel composite

89 material was used to fabricate a thermal sensor capable of degrading within a 48-hour window  
90 under ideal conditions.

91

## 92 EXPERIMENTAL SECTION

### 93 *General Information.*

94 PCL (Mn 45,000, m.p. 56–64 °C, MFI 1.8 g/10 min at 80 °C, 44 psi), Amano Lipase PS from  
95 *Burkholderia cepacia* ( $\geq 10,000$  U/g, opt. pH and temperature 7.0 & 50 °C, protein ~1.0 wt.%), 1-  
96 pyrenebutyric acid (PBA), 1-Ethyl-3-dimethylaminopropyl carbodiimide (EDC), carboxymethyl  
97 cellulose, monosodium phosphate ( $\text{NaH}_2\text{PO}_4$ ), and disodium phosphate ( $\text{Na}_2\text{HPO}_4$ ) were  
98 purchased from Sigma-Aldrich. Organic solvents, methanol and dimethyl sulfoxide (DMSO) were  
99 purchased from Merck. Sodium phosphate buffer (0.10 M, pH 7.5) was prepared via a standard  
100 recipe.<sup>34</sup> CNF (PR-24-XT-LHT-OX; avg. diameter ~150 nm, length ~50–200  $\mu\text{m}$ , aspect ratio ca.  
101 ~300–1300, surface area ~20–30  $\text{m}^2/\text{g}$ ) were procured from Pyrograf (Cedarville, USA). All  
102 materials were used as received except for polycaprolactone which was cryoground to a fine  
103 powder (sieved,  $\leq 300$   $\mu\text{m}$ ). To ensure adequate heating and uniform mixing of samples during  
104 degradation experiments an orbital incubating shaker (Lab Companion SI600R; Yuseong-gu,  
105 Daejeon, Korea) was used. Thermal pressing of sample films was performed on a hot press  
106 (Siempelkamp; Krefeld, DE) and sensing patterns were cut by laser scribing using a commercial  
107  $\text{CO}_2$  laser engraving machine (Makerspace G640L; NZ) with a laser power of 15 W and scan rate  
108 of 100 mm/s.

109

### 110 *Characterization.*

111 The electrical performance of CNF (pristine and functionalized) and subsequent PCL  
112 composites was measured using a multimeter (Limit 500). The resistances of commercial and  
113 functionalized CNFs were measured as a dried dispersion in carboxymethyl cellulose (1.0 wt.%)  
114 over a distance of 20 mm to allow for direct comparison between treatment methods. The  
115 conductivities of PCL composite films (10 mm x 12 mm) were measured at a distance of 12 mm  
116 with silver ink at the interface to reduce contact resistance. For temperature sensing measurements  
117 real time electrical resistance changes of sensor electrodes were recorded using an LCR meter (IM  
118 3536 Hioki; Japan) with an applied voltage of 1.00 V. To measure the change in pH during  
119 degradation and titration experiments a pH probe (Seven Compact, Mettler Toledo; USA)  
120 equipped with an Ag/AgCl electrode was used. The surface and cross-sectional microstructures of  
121 CNFs (pristine and functionalized) and PCL-based composites (before/after degradation) were  
122 investigated via field emission scanning electron microscopy (FE-SEM) (JSM 6700 JEOL; Japan).  
123 Samples were sputter coated with chromium (10.0 nm thickness) and analyzed at an accelerating  
124 voltage of 3.00 kV. To measure the crystallinity of PCL and PCL-based composites differential  
125 scanning calorimetry (DSC) was performed in heat-cool-heat mode by a Discovery DSC (TA  
126 Instruments) equipped with a refrigerated cooling system. Samples (5.00 mg) were placed in a  
127 TZero aluminum pan under nitrogen (10 mL/min) and the temperature cycle: equilibration at  
128  $-80.00\text{ }^{\circ}\text{C}$ ; isothermal 5.00 min; ramp  $10.00\text{ }^{\circ}\text{C}/\text{min}$  to  $80.00\text{ }^{\circ}\text{C}$ ; ramp  $5.00\text{ }^{\circ}\text{C}/\text{min}$  to  $-80.00\text{ }^{\circ}\text{C}$ ;  
129 isothermal 5.00 min; ramp  $10.00\text{ }^{\circ}\text{C}/\text{min}$  to  $80.00\text{ }^{\circ}\text{C}$  was used. Data from the second heating scan  
130 was used for the analysis. Thermogravimetric analysis (TGA) was carried out on a TGA1-0329  
131 instrument (TA Instruments, USA), using a heating ramp of  $10.0^{\circ}\text{C}/\text{min}$  under a  $\text{N}_2$  atmosphere.  
132 Liquid chromatography-mass spectrometry (LCMS) was performed using an Agilent Series 1290  
133 HPLC (Agilent Technologies, Santa Clara, CA) equipped with a reverse phase C18 analytical

134 column of 150 mm × 3.0 mm and 2.7 μm particle size (Poroshell 120 EC-C18). Chemical surface  
135 analysis was carried out using a Kratos AXIS DLD X-ray photoelectron spectrometer (XPS)  
136 equipped with a hemispherical electron energy analyzer. For sample excitation, a monochromatic  
137 Al Kα source (1486 eV, 150 W) was used, and survey scans were collected (160 eV pass energy),  
138 followed by core level scans for O, N and C. The analysis chamber was evacuated to pressures in  
139 the range of  $1.3 \cdot 10^{-9}$  mbar. Data analysis was carried out using the Casa XPS software; relative  
140 sensitivity factors for the elements were used as supplied with the instrument. For electrically  
141 conductive samples, no charge correction was applied. Non-conductive samples were referenced  
142 to 284.8 eV for their C1s peak. Background correction was done using Shirley backgrounds. For  
143 the core scan data, graphite was used as the reference material. Enzyme activity measurements  
144 were performed using a standard p-nitrophenol assay at room temperature.

145

146 *Immobilization of lipase (AL) onto CNF.*

147 a)  $CNF_{PBA}$ —The immobilization of lipase on to CNF was adapted and modified from literature.<sup>35</sup>  
148 CNFs (1.00 g) were dispersed in DMSO (35.0 mL) and sonicated for 1 hour at 25 °C. The  
149 dispersion was then transferred to a 50.0 mL centrifuge tube where 1-pyrenebutyric acid (PBA)  
150 (1.18 g) and an additional 5.00 mL of DMSO were added. The mixture was shaken for 3 hours (25  
151 °C, RCF = 1.05 x g) and then centrifuged for 10 min (18 °C, RCF = 3184 x g). The supernatant  
152 was then decanted, and the remaining black solids were washed and centrifuged with methanol  
153 and then water. After washing, the remaining solids were freeze dried and recovered. The total  
154 weight fraction of bound PBA was found to be 10.0% by titration, Yield 1.10 g.

155 b)  $CNF_{AL}$ —PBA functionalized CNFs (0.764 g) were dispersed in phosphate buffer (90.0 mL,  
156 pH 7.2, 50.0 mM) and sonicated for 1 hour at 25 °C. Then, additional buffer (20.0 mL) and EDC

157 (3.34 g) were added, and the mixture was shaken for 30 min (25 °C, RCF = 1.05 x g). The reaction  
158 mixture was then centrifuged for 10 min, decanted, and the remaining black solid was washed with  
159 additional buffer via centrifugation. The activated black solid was again dispersed in fresh  
160 phosphate buffer (20.0 mL, pH 6.5, 50.0 mM) and 75.0 mL of lipase solution in buffer (9000 U,  
161 pH 6.5) was added. The mixture was then shaken for 30 min (RCF = 1.05 x g), centrifuged, and  
162 then washed with methanol and then water and freeze dried. The immobilized material was found  
163 to have an activity of 0.720 U/mg and the immobilization yield was found to be 4.60% (see  
164 Supporting Information). Yield 0.514 g

165

166 *General procedure for the preparation of fast-degrading conductive composites.*

167 CNF<sub>AL</sub>-PCL. Ground PCL was dried at 40 °C in a vacuum oven for two days and then manually  
168 mixed with AL functionalized CNF (CNF<sub>AL</sub>) in a PTFE coated vessel at 75 °C maintaining a 20.0  
169 wt.% ratio of CNF<sub>AL</sub> to PCL. The compounded mixtures were then hot pressed between PTFE  
170 coated steel plates at 75 °C for 1 min at 50.0 kN, followed by 1 min at 30.0 kN to a thickness of  
171 600 μm. To achieve a smooth surface all films were pressed and repressed at least two times. An  
172 additional film CNF-AL<sub>5</sub>-PCL, containing un-immobilized (free) AL powder, pristine CNF, &  
173 PCL and control films containing CNF-PCL (no enzyme), AL<sub>x</sub>-PCL (x = 1.00, 5.00%; no CNF),  
174 and pure PCL were also fabricated. See Table 1. and Supporting Information for weight ratios and  
175 composition. Weight percentages for AL are based on the unpurified powder. All films were then  
176 analyzed by FE-SEM, DSC, TGA, and for their electrical performance. Samples were stored in a  
177 desiccator prior to use.

178

179 *Degradation of fast-degrading conductive composites.*

180 CNF<sub>AL</sub>-PCL film and control samples (40.0 mg) were placed into glass scintillation vials  
181 containing phosphate buffer (2.00 mg/mL film to buffer; pH 8.0, 0.100 M) and capped with a  
182 PTFE-lined screw cap. The samples were placed in an orbital incubator shaker and maintained at  
183 a temperature of 50 °C and shaken at RCF = 1.05 x g for up to 24 days or until full degradation.  
184 Samples of each film were prepared in triplicate for each time point observed and consumed. At  
185 the end of each time point the degradation mixture was carefully transferred and centrifuged at  
186 RCF = 3184 x g for 10 min. The supernatant was decanted, freeze dried, and analyzed by LCMS,  
187 while the collected residue was washed repeatedly with deionized water and recollected by  
188 centrifugation, freeze dried and weighed to obtain the total percent weight loss (Wt.<sub>avg</sub>%).  
189 Undegraded plastic film residue from selected time points were then analyzed by FE-SEM.

190

191 *Degradation of fast-degrading thermal sensor.*

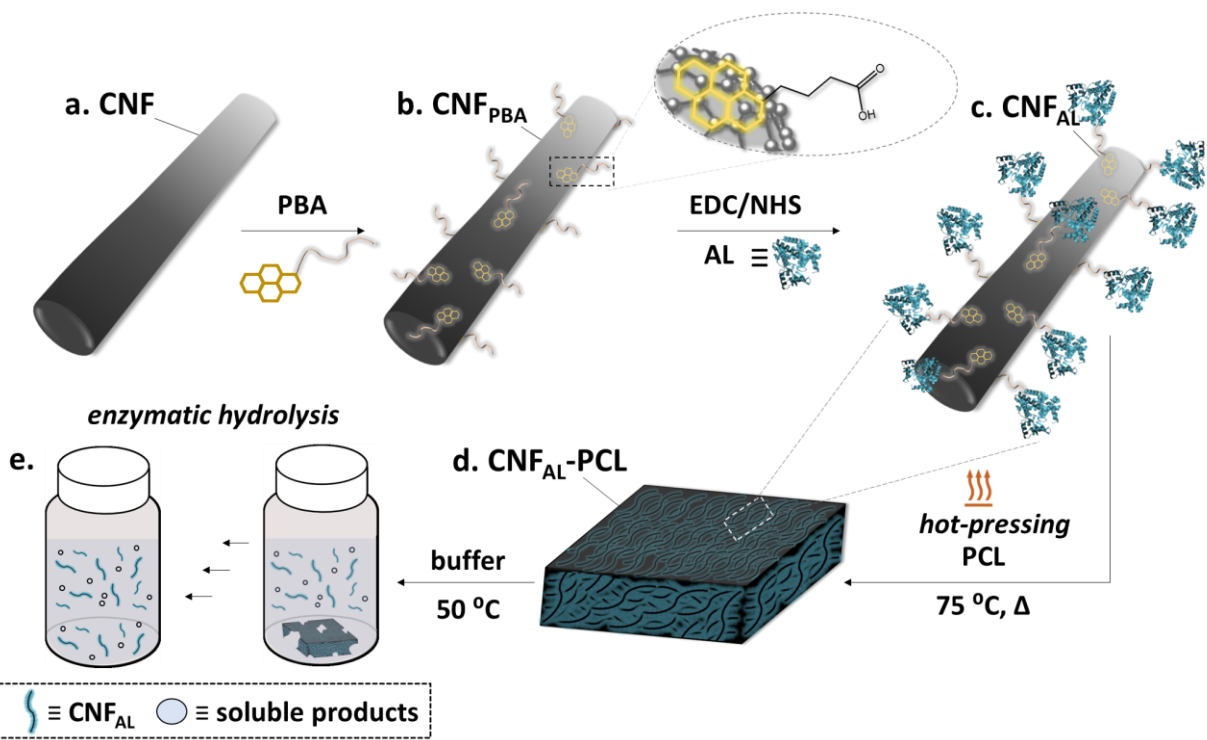
192 A thermal sensor composed of [CNF<sub>AL</sub>-PCL/AL<sub>5</sub>-PCL] was placed into a 200 mL beaker and  
193 phosphate buffer (2.00 mg/mL film to buffer; pH 8.0, 0.100 M) was added and the beaker was  
194 tightly secured and covered with aluminum foil. The bottles containing the sensor and buffer  
195 solution were then placed in an orbital incubator shaker at 50 °C (RCF = 1.05 x g) and were  
196 degraded over a period of 48 hours.

197

198

199

200

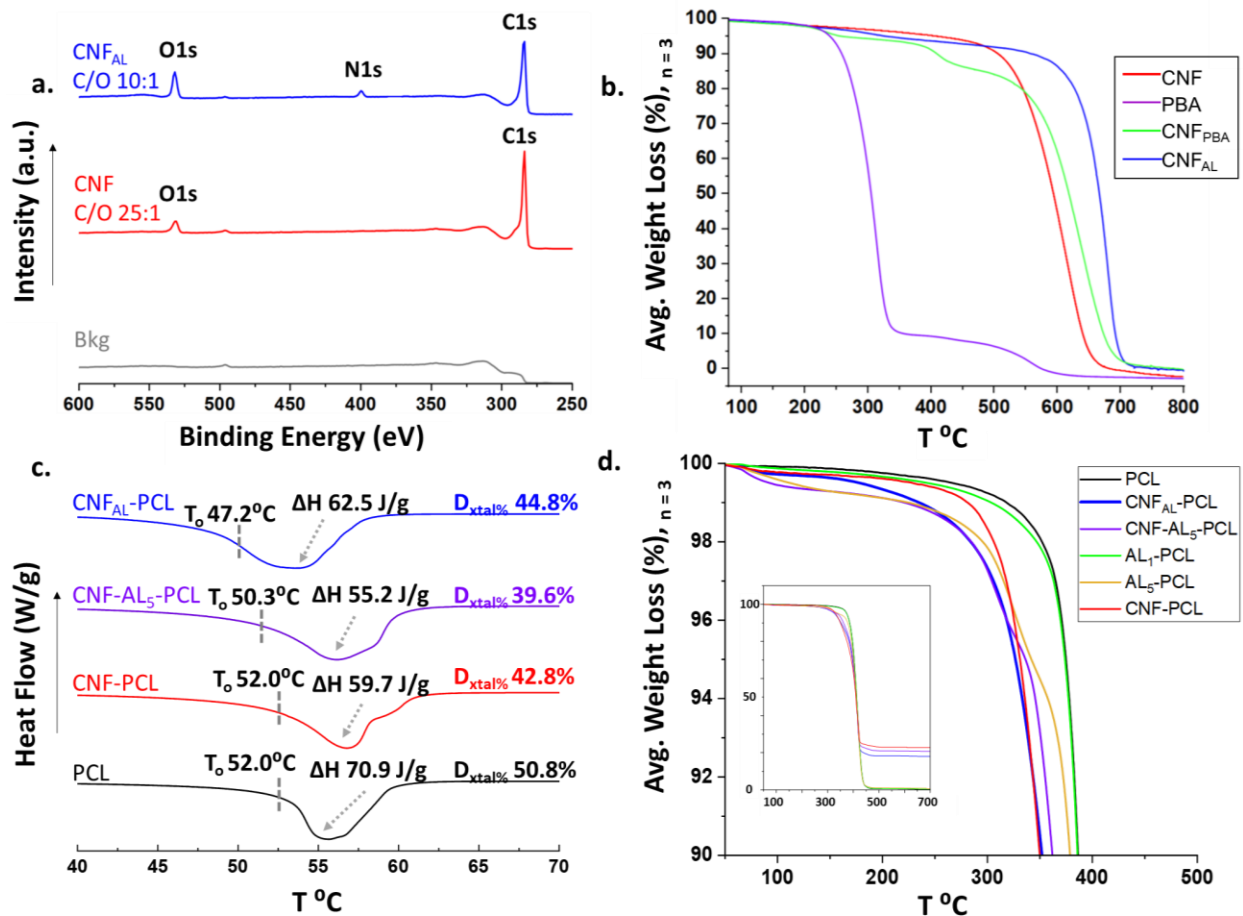


201  
 202 **Figure 1.** Graphical representation of the manufacturing process and compounding of a fast-  
 203 degrading conductive composite. a) Pristine carbon CNF are first reacted with PBA to form b)  
 204 CNF<sub>PBA</sub>. CNF<sub>PBA</sub> is then coupled to AL via EDC/NHS coupling to form c) CNF<sub>AL</sub>. CNF<sub>AL</sub> is then  
 205 hot pressed at 60 °C with PCL to form the fast-degrading conductive composite, d.) CNF<sub>AL</sub>-PCL  
 206 conductive composite e) the enzymatic hydrolysis of CNF<sub>AL</sub>-PCL via embedded CNF<sub>AL</sub> in buffer  
 207 at 50 °C with agitation.

208  
 209 **RESULTS AND DISCUSSION**

210 In this study we describe the preparation, fabrication, and enzyme-mediated rapid degradation  
 211 of environmentally benign conductive thermoplastic composites. To prepare these materials CNFs  
 212 were functionalized with a polyester-degrading lipase, AL, and these enzyme-coated fibers were  
 213 then compounded with the biodegradable polyester PCL which serves as the thermoplastic matrix  
 214 to be enzymatically degraded (Figure 1a-e.). Additionally, to demonstrate the viability of these

215 composites for use in electronic sensing devices a thermal sensor was fabricated, characterized,  
 216 and finally degraded as a proof-of-concept.



217  
 218 **Figure 2.** a.) XPS of AL immobilized carbon nanofibers ( $\text{CNF}_{\text{AL}}$ ) and pristine CNF. b.) TGA  
 219 showing the average weight loss percentage of  $\text{CNF}_{\text{PBA}}$ ,  $\text{CNF}_{\text{AL}}$ , pristine CNF, & PBA. c.) DSC  
 220 showing the percent crystallinity ( $D_{\text{xtal}}\%$ ), melting onset temperature ( $T_o$ ) and heat of fusion ( $\Delta H$ )  
 221 of  $\text{CNF}_{\text{AL}}\text{-PCL}$ ,  $\text{CNF-AL}_5\text{-PCL}$ ,  $\text{CNF-PCL}$ , & PCL composite films. d.) TGA showing the average  
 222 weight loss percentage of the composite films  $\text{CNF}_{\text{AL}}\text{-PCL}$ ,  $\text{CNF-AL}_5\text{-PCL}$ , and the positive and  
 223 negative controls.

224  
 225

226

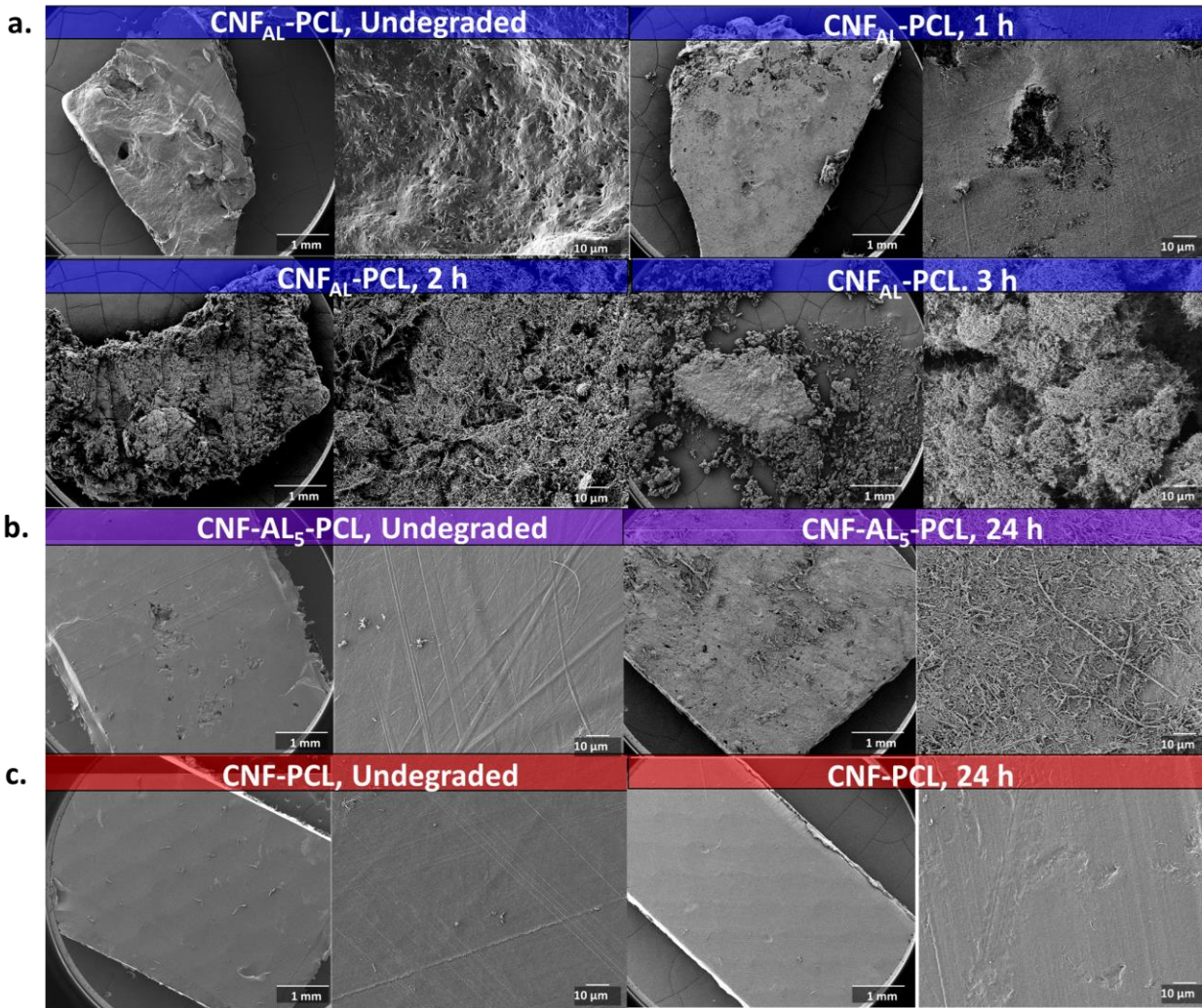
### 227 *Immobilization of AL onto CNF*

228 A modified procedure<sup>35</sup> from Min et al. was used to immobilize AL onto CNF via an  
229 intermediate linking step with 1-pyrenebutyric acid (PBA). Pristine CNF was initially reacted with  
230 PBA through supramolecular  $\pi - \pi$  interactions between the surface of the CNF and the aromatic  
231 pyrene system (Figure 1a & b). To measure the amount of PBA immobilized onto CNF, a titration  
232 was performed by dispersing the resultant CNF<sub>PBA</sub> material into dilute NaOH and titrating the  
233 deprotected COO<sup>-</sup> groups with dilute HCl (Table S1.). From the titration it was determined that  
234 CNF<sub>PBA</sub> contained ~10.0% PBA by weight. To complete the immobilization of AL onto CNF,  
235 CNF<sub>PBA</sub> was then reacted with AL via a standard EDC coupling to form the conductive biocatalyst  
236 CNF<sub>AL</sub> (Figure 1c).<sup>36</sup> The activity of the resulting immobilized CNF<sub>AL</sub> material was found to be  
237 0.720 U/mg after reaction with p-nitrophenol and the calculated immobilization yield was found  
238 to be 4.10%.

$$239 \quad (a) \text{ immobilization yield} = \frac{\text{immobilized activity}}{\text{starting activity of free enzyme}}$$

240 Further characterization of CNF<sub>AL</sub> was also performed using X-ray photoelectron spectroscopy  
241 (XPS) (Figure 2a.). Analyzing the resulting peaks from pristine CNF and CNF<sub>AL</sub> both show a  
242 strong C1s peak from 284-290 eV and a slightly weaker peak for O1s at ~531 eV, however only  
243 CNF<sub>AL</sub> shows a peak for N1s. The C/O ratios for CNF and CNF<sub>AL</sub> are 25:1 and 10:1, respectively,  
244 and the C/N ratio for CNF<sub>AL</sub> is 33:1, which is in line with the enzyme being immobilized to the  
245 substrate as AL is the only apparent nitrogen source. Thermal gravimetric analysis (TGA) was also  
246 conducted on CNF, PBA, CNF<sub>PBA</sub>, and CNF<sub>AL</sub> (Figure 2b.). The degradation curve of pristine  
247 CNF shows a 98.0% weight loss between 550-650 °C, which is attributed to the degradation of the  
248 CNF material itself. The weight loss data of CNF<sub>AL</sub>, however, shows an initial ~5.0% loss between

249 ~300-400 °C and then a 95.0% weight loss between ~650-700 °C. From analyzing the other  
250 samples this 5.00% loss is possibly due to hydrogen bound water or other impurities as it is also  
251 present in CNF<sub>PBA</sub>, but not in pristine CNF. In CNF<sub>PBA</sub>, the degradation of PBA occurs between  
252 400-500 °C, as shown by a ~10.0% weight loss which matches well with titration experiments.  
253 This weight loss is not present in CNF<sub>AL</sub> meaning that bound PBA is stabilized and protected via  
254 conjugation with the enzyme. Additionally, the degradation of CNF is delayed by about ~100 °C  
255 due to this conjugation, as compared with pristine CNF. As for the electrical performance of  
256 CNF<sub>AL</sub>, it was found to have a resistance of  $600 \pm 126 \Omega$  compared to  $575 \pm 140 \Omega$  for pristine  
257 CNF, both determined using an equal amount of sample dispersed over an equal surface area, to  
258 allow direct quantitative comparison (Table S2.). Analyzing the data there appears to be no  
259 significant change in resistance of CNF post functionalization.



260

261 **Figure 3.** a.) Scanning electron microscope (SEM) images of CNF<sub>AL</sub>-PCL undegraded film and  
 262 after 1, 2, & 3 hours of degradation. b.) Images of CNF-AL<sub>5</sub>-PCL and c.) CNF-PCL undegraded  
 263 film and after 24 hours of degradation.

264 *Fabrication of fast-degrading conductive composites*

265 Composites containing CNF and PCL with no AL were first compounded and hot-pressed  
 266 to a thickness of 600 μm at different weight percentages of CNF in PCL (5.00, 10.0, 15.0, 20.0, &  
 267 30.0 wt.%) and the conductivity of each material was measured (Figure S1.). This was to determine  
 268 the minimum amount of CNF needed to ensure the highest level of performance, while maintaining

269 structural integrity. It was found that 20.0% CNF was the maximum amount of CNF that could be  
270 added to the composite before the conductivity begins to level off producing diminishing returns  
271 (Figure S1a.). Once this had been determined, composites containing CNF<sub>AL</sub> and PCL were  
272 fabricated in a similar manner to produce the fast-degrading conductive thermoplastic material,  
273 CNF<sub>AL</sub>-PCL. The total composition of CNF<sub>AL</sub>-PCL was found to be 20.0 % CNF<sub>AL</sub> and 80.0 %  
274 PCL with a total activity per weight added of 14.4 U/100 mg of composite (Table 1.). To  
275 understand how immobilization of AL effects the degradation of the material another set of  
276 composites were fabricated containing CNF, PCL, and un-immobilized AL powder, CNF-AL<sub>x</sub>-  
277 PCL (x = 1.00 or 5.00 wt.% AL powder; 10.0 U/100 mg & 50.0 U/100 mg, respectively). These  
278 compositions were chosen as it has been previously demonstrated that these percentages of AL  
279 powder in PCL with no CNF present are very effective at degrading PCL,<sup>15</sup> however preliminary  
280 degradation studies showed no degradation activity present in CNF-AL<sub>1</sub>-PCL after 24 days, so the  
281 study was continued only using CNF-AL<sub>5</sub>-PCL. In addition to CNF<sub>AL</sub>-PCL and CNF-AL<sub>5</sub>-PCL,  
282 an assortment of positive and negative controls was also fabricated including CNF-PCL, where no  
283 AL is present, and AL<sub>x</sub>-PCL (x = 1.00 or 5.00 wt.% AL powder; 10.0 U/100 mg & 50.0 U/100  
284 mg, respectively) where no CNF is present (see Tables 1. and S3. for composition data). The  
285 conductivity of PCL-based CNF composites decreases with the addition of AL, this is an expected  
286 result as AL is not an electrically conductive material. Experimental measurements demonstrate  
287 that CNF-PCL has the highest conductivity at  $31.0 \pm 6$  S/m and CNF<sub>AL</sub>-PCL and CNF-AL<sub>5</sub>-PCL  
288 have a similar conductivity at  $14.0 \pm 2$  S/m and  $22.0 \pm 5$  S/m, respectively (Table 1.).

289

290

291 **Table 1.** Composition and conductivity of PCL/CNF-based composites

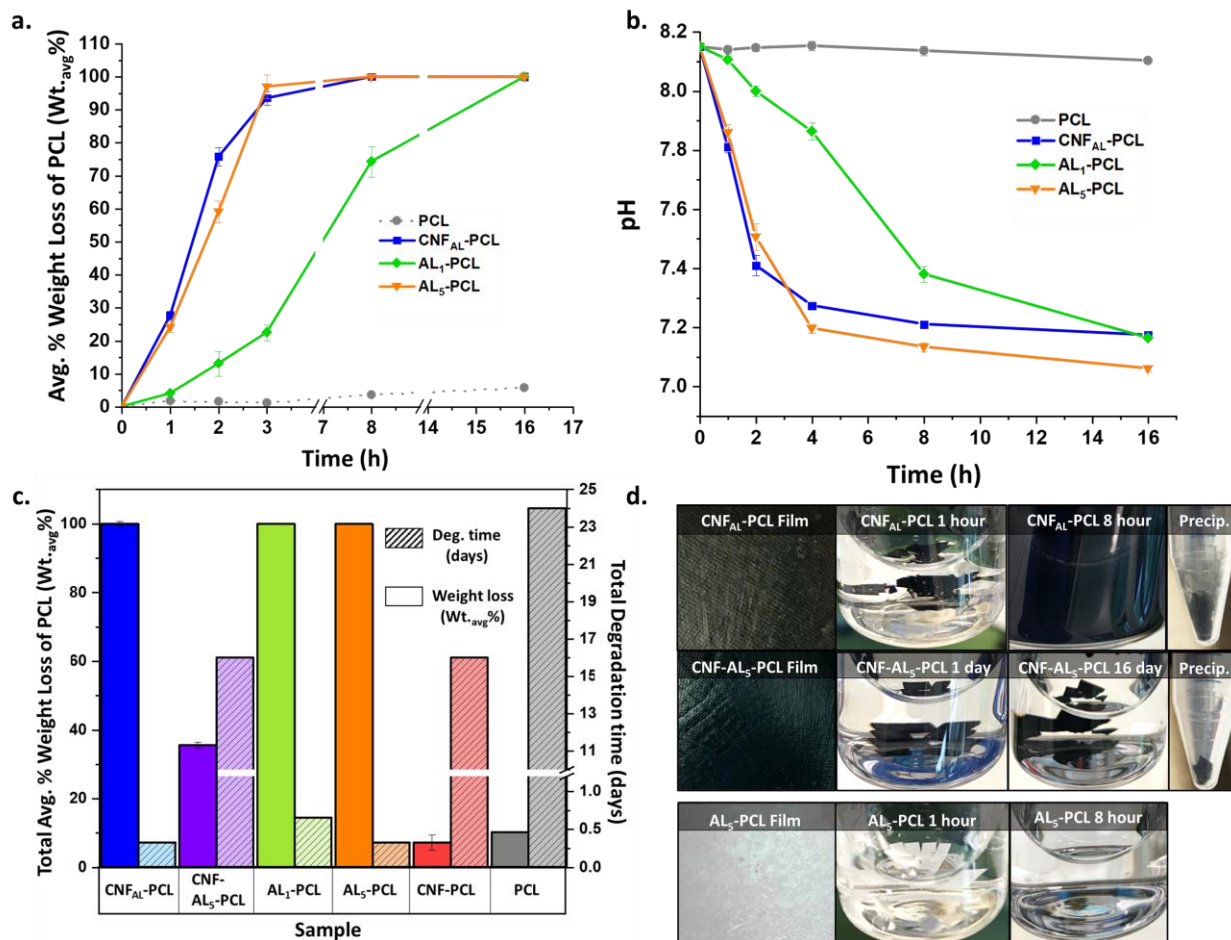
Sample	PCL (wt.%)	CNF (wt.%)	CNF <sub>AL</sub> (wt.%)	AL powder (wt.%)	Activity (U) /100 mg	Conductivity (S/m)
CNF <sub>AL</sub> -PCL	80.0	–	20.0	–	14.4	14.0 ± 2
CNF-AL <sub>5</sub> -PCL	75.8	19.2	–	5.02	50.0	22.0 ± 5
CNF-PCL	81.0	19.2	–	–	–	31.0 ± 6
PCL	100	–	–	–	–	–

292 *\*Values rounded to three significant figures.*

293 DSC and TGA were performed to investigate the thermal properties of the composites  
 294 (Figure 2c-d). PCL is known to exist in a variety of phases, including fully crystalline and plastic  
 295 crystal mesophases,<sup>37</sup> the presence and extent of which depend on the processing conditions. For  
 296 pure PCL both the degree of crystallinity and onset of melting temperature (50.8 % and 52.0 °C  
 297 respectively) are highest among all the composites, except for CNF-PCL where the onset of  
 298 melting temperature is the same. The melting behavior of pure PCL is also characterized by a  
 299 single peak, indicating the presence of one predominant type of crystallites. By contrast, CNF-  
 300 PCL and CNF-AL<sub>5</sub>-PCL display melting transitions that clearly represent two distinct processes,  
 301 and correspondingly, the presence of two different types of crystalline phases. The total degree of  
 302 crystallinity is lower for both (42.8 % and 39.6 %, respectively), while the onset of melting is  
 303 shifted down by a few °C. Since both composites contain non-functionalized CNF, it is likely that  
 304 this change in the PCL matrix is caused by the influence the bare CNF surfaces have on the  
 305 polymer crystallization (e. g., through nucleation and/or stabilization of a different phase). CNF<sub>AL</sub>-  
 306 PCL, however, shows a single melting peak with an even lower onset temperature and an  
 307 intermediate degree of crystallinity (44.8 %). Since the CNF present in this material are decorated  
 308 with enzyme, their surface properties can be expected to significantly differ from non-  
 309 functionalized CNF which in turn is likely to lead to a different effect on the crystallization process  
 310 of the PCL. A different phase composition of the crystalline domains in the various composites

311 can be assumed to be the reason for the qualitatively observed brittleness of CNF<sub>AL</sub>-PCL versus  
312 the other composites. Thermal gravimetric analysis (TGA) revealed that the degradation profiles  
313 observed for all composites aligns well with their reported compositions (Figure 2d.). All  
314 composites containing CNF report a ~75.0–80.0% weight loss between 350–400 °C, which  
315 accounts for the loss of the PCL polymer matrix. CNF<sub>AL</sub>-PCL and CNF-PCL also share a similar  
316 degradation profile except for a small weight loss for CNF<sub>AL</sub>-PCL between 175–300 °C, which  
317 can be reasonably attributed to either hydrogen bound water and/or PBA and immobilized AL.  
318 Similarly, CNF-AL<sub>5</sub>-PCL and AL<sub>5</sub>-PCL both show a ~5.00% weight loss between 100–300 °C  
319 which can be attributed to the loss of free AL powder. To investigate the surface and cross-  
320 sectional morphologies SEM images were captured for all composites prior to degradation. The  
321 surface of undegraded CNF<sub>AL</sub>-PCL (Figure 3a.) is rather uneven in nature and it is evident at high  
322 magnification that CNFs immobilized with AL are present on the surface forming a patchwork-  
323 like pattern in the plastic. In contrast, CNF-AL<sub>5</sub>-PCL and CNF-PCL seem to have a far smoother  
324 contiguous surface with little to no CNF (pristine) present even at high magnification (Figure S2.).  
325 Analyzing the cross-sectional images, CNF is visible in all three composites and there is no  
326 indication of increased bundling, clustering, or alignment of CNF. However, it is noted that the  
327 polymer matrix of CNF-PCL and CNF-AL<sub>5</sub>-PCL display a grainy structure in cross-section which  
328 was also found in pure PCL (Figure S3.). It was absent, however, in CNF<sub>AL</sub>-PCL, which correlates  
329 well with DSC results as CNF<sub>AL</sub>-PCL is shown to have a different crystalline phase that results in  
330 a lower melting temperature. Additionally, AL was also found to be well distributed throughout  
331 the composite as evidenced via fluorescence microscopy with fluorescein tagged AL (Figure S4.).  
332 Dynamic mechanical thermal analysis (DMTA) was undertaken to quantify the difference in  
333 mechanical properties between the composites, however, due to the brittleness of CNF<sub>AL</sub>-PCL the

334 results were inconclusive. Although CNF<sub>AL</sub>-PCL is rather brittle this does not prevent the material  
 335 from being deployed in small sensors or other electronic devices that are fit-for-purpose and that  
 336 are not subject to high mechanical loads.



337  
 338 **Figure 4.** a.) The average percent weight loss (Wt.<sub>avg</sub>%) of CNF<sub>AL</sub>-PCL and control films at 50 °C,  
 339 RCF = 1.05 x g, over 16 hours. b.) Change in pH of buffer during 16-hour degradation of CNF<sub>AL</sub>-  
 340 PCL and control films. c.) Histogram depicting the time (Deg. time) that each composite film takes  
 341 before no further degradation is observed and total avg. weight loss percent achieved during that  
 342 period. d.) Pictures of CNF<sub>AL</sub>-PCL, CNF-AL<sub>5</sub>-PCL, and AL<sub>5</sub>-PCL during various stages of the  
 343 degradation process.

344 *Degradation Trials*

345 To test the degradation capabilities of CNF<sub>AL</sub>-PCL and CNF-AL<sub>5</sub>-PCL, under ideal conditions,  
346 40.0 mg rectangular films with a thickness of ~600 μm were cut and submerged in basic phosphate  
347 buffer (plastic to buffer ratio 2.00 mg/mL). The films were heated and shaken at 50 °C and 2 RCF  
348 = 1.05 x g. This procedure was also performed for the positive controls AL<sub>1</sub>-PCL and AL<sub>5</sub>-PCL  
349 and for negative controls CNF-PCL and PCL. Sacrificial samples were made for each selected  
350 timepoint to measure how the films degrade over time and the films were kept under degradation  
351 conditions for a maximum of 24 days or until full degradation and dissolution of degradation  
352 products occurred. For degraded samples containing CNF special care was taken to disambiguate  
353 liberated CNF from undegraded PCL film by centrifuging the terminal samples after each  
354 timepoint measured. PCL film is denser than CNF and sinks to the bottom of the centrifuge tube,  
355 while CNF floats to the top as a finely dispersed particulate. As the degradation experiments  
356 progressed it was immediately evident that the degradation activity between CNF<sub>AL</sub>-PCL and  
357 CNF-AL<sub>5</sub>-PCL occurred on vastly different timescales with CNF<sub>AL</sub>-PCL degrading rapidly in a  
358 matter of hours while full degradation of CNF-AL<sub>5</sub>-PCL failed to occur even after 24 days. Figures  
359 4a. and S5. show the average percent weight loss of PCL (Wt.<sub>avg</sub>%) for CNF<sub>AL</sub>-PCL, the positive  
360 controls, and PCL over a 16-hour period. Within the first hour the Wt.<sub>avg</sub>% for CNF<sub>AL</sub>-PCL was  
361 around 30.0% and astonishingly after the third hour it was at 90.0% total PCL weight loss. The  
362 degradation profile of CNF<sub>AL</sub>-PCL tracks well with the positive control AL<sub>5</sub>-PCL which is even  
363 more impressive as CNF<sub>AL</sub>-PCL has a lower activity per mass ratio than AL<sub>5</sub>-PCL, 14.0 U vs. 50.0  
364 U mg present per 100 mg of composite, respectively, and since AL<sub>5</sub>-PCL was specifically  
365 fabricated to be a fast-degrading formulation. In total it takes CNF<sub>AL</sub>-PCL and AL<sub>5</sub>-PCL eight  
366 hours to fully degrade, while AL<sub>1</sub>-PCL, which has an activity of 10.0 U/100 mg of composite,

367 takes 16 hours for full disintegration and dissolution. To get a more complete understanding of  
 368 what degradation products were formed during this experiment aliquots of the supernatant were  
 369 analyzed by LCMS after three hours for CNF<sub>AL</sub>-PCL, AL<sub>1</sub>-PCL, and AL<sub>5</sub>-PCL (Table 2.). For  
 370 CNF<sub>AL</sub>-PCL it was found that most degradation products had molecular weights below ~1000 Da  
 371 with 63.0% between ~500–1000 Da and 18.4% below ~500 Da. Only a small percentage of  
 372 products, 18.7%, were found to be between ~1000–2000 Da. As for the positive controls, the  
 373 fastest degrading film AL<sub>5</sub>-PCL was found to have most of its degradation products below ~500  
 374 Da, 66.0%, with only 33.2% between ~500–100 Da, and < 1.00% over 1000 Da.

375 **Table 2.** Percent distribution of molecular weights (D%) after degradation (3 hr)

Sample	<500 (Da)	500-1000 (Da)	1000-2000 (Da)
CNF <sub>AL</sub> -PCL	18.4	63.0	18.7
AL <sub>1</sub> -PCL	16.2	58.0	25.8
AL <sub>5</sub> -PCL	66.0	33.2	0.860

376 *\*Values rounded to three significant figures.*

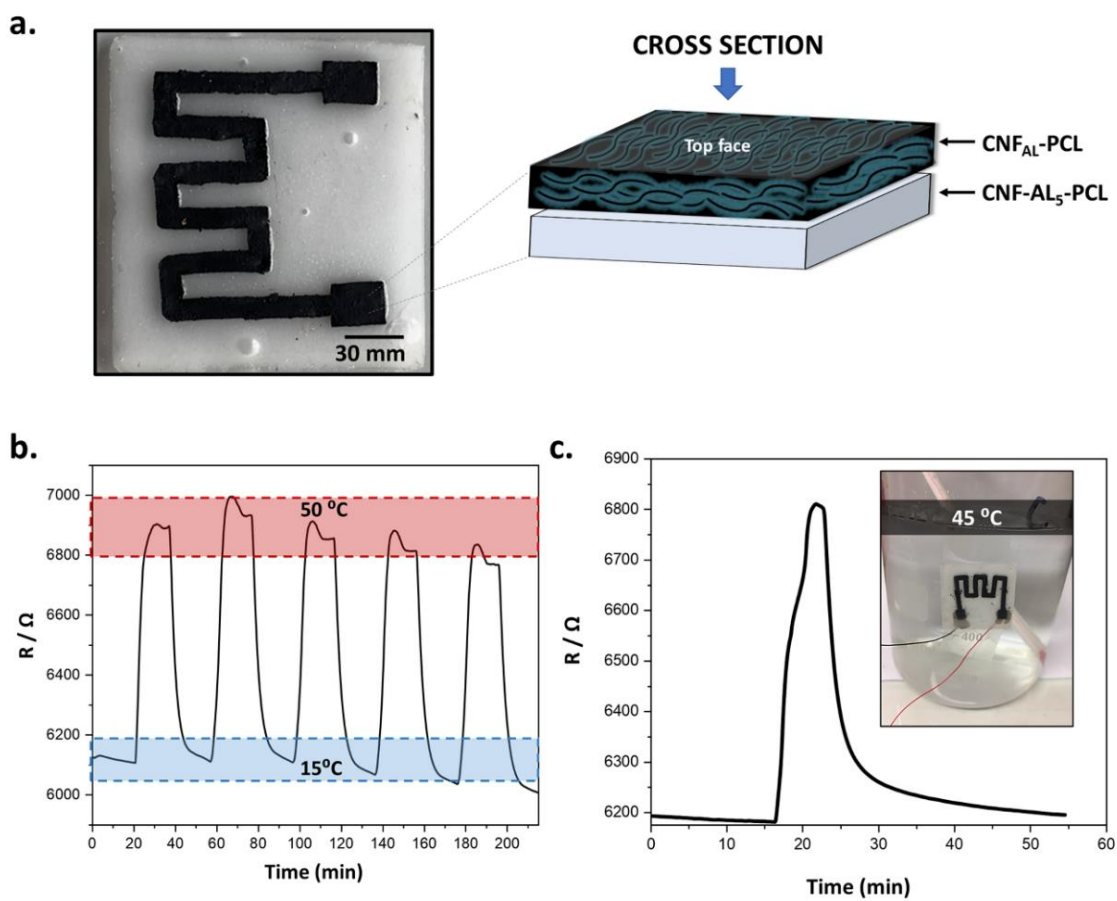
377 AL<sub>1</sub>-PCL showed a degradation product molecular weight distribution more similar to CNF<sub>AL</sub>-  
 378 PCL after three hours with the majority of its products between ~500–100 Da. In addition to the  
 379 50 °C degradation experiments, CNF<sub>AL</sub>-PCL composites were also degraded at 30 °C (Figure S6b.)  
 380 to understand how AL performed below of its optimum temperature. It was found that after 14  
 381 days CNF<sub>AL</sub>-PCL composites of a similar size showed a Wt.<sub>avg</sub>% of 50.0%, which is still much  
 382 faster than CNF-AL<sub>5</sub>-PCL at 50.0 °C. When PCL is hydrolyzed by AL soluble acidic oligomers  
 383 and 6-hydroxyhexanoic acid are produced, which lower the pH of the overall degradation media.  
 384 In addition to measuring the Wt.<sub>avg</sub>% for CNF<sub>AL</sub>-PCL and the control films, the pH was also  
 385 monitored during the 16-hour degradation period (Figure 4b.). The pH trace for CNF<sub>AL</sub>-PCL and  
 386 AL<sub>5</sub>-PCL also track similarly with a pH drop around ~0.3 units after the first hour and ~0.6 units  
 387 after the second hour, after two hours the drop in pH begins to slow down and eventually levels

388 off after eight hours. For AL<sub>1</sub>-PCL this decrease also tracks the degradation of the film with a slow  
389 drop in pH for the first 4 hours and then a much larger drop around eight hours and eventually  
390 falling to the level of CNF<sub>AL</sub>-PCL and AL<sub>5</sub>-PCL (Figure 4b.).

391

392 SEM images were also taken of CNF<sub>AL</sub>-PCL and CNF-AL<sub>5</sub>-PCL at different points during  
393 degradation to analyze the surface and cross-sectional morphologies of actively degrading films  
394 (Figures 3a-b. & S2.). SEM images of the fast-degrading CNF<sub>AL</sub>-PCL were taken every hour  
395 during the first three hours of degradation and images of CNF-AL<sub>5</sub>-PCL were taken after the first  
396 24 hours of degradation. Analyzing the images of CNF<sub>AL</sub>-PCL during the first hour of degradation  
397 it was already apparent that the volume of PCL was beginning to lessen as the presence of CNF  
398 fibers becomes exaggerated at the surface. Additionally, large gaps in the film, which are formed  
399 when the PCL matrix is degraded from the inside out, via an embedded enzyme, are beginning to  
400 form after the second hour. It is surmised that these large gaps greatly increase the speed of  
401 degradation as new channels are formed throughout the plastic giving rise to the activation of  
402 deeply embedded AL by water. After the third hour the PCL seems to have mostly degraded  
403 demonstrating a total loss in integrity in the film. This contrasts with the images of the CNF-AL<sub>5</sub>-  
404 PCL film, which were taken after 24 hours, that appear to only be slightly eroded at the surface.  
405 Figure 4c. shows the amount of time that each composite film takes before no further degradation  
406 is observed and the total weight loss achieved during that period. CNF-AL<sub>5</sub>-PCL degrades for 16  
407 days until a final weight loss average of 34.0% is achieved, while the negative controls CNF-PCL  
408 and PCL also take 16 days to reach a final weight loss of 7.00% and 9.00%, respectively. The  
409 drastic difference in degradation speed between CNF<sub>AL</sub>-PCL and CNF-AL<sub>5</sub>-PCL can be majorly  
410 attributed to the lack of open channels on the surface of CNF-AL<sub>5</sub>-PCL that allow for water to

411 enter the plastic matrix thereby “activating AL.” Another major reason is that CNF<sub>AL</sub>-PCL is more  
 412 brittle than CNF-AL<sub>5</sub>-PCL and has a higher propensity to fracture during the degradation process  
 413 exposing more surfaces to an aqueous environment speeding up degradation of the plastic. CNF-  
 414 PCL was found to be the lowest performing composite film overall which suggests that the addition  
 415 of the hydrophobic pristine CNF to the PCL matrix may reduce the efficiency of the un-mediated  
 416 hydrolysis reaction, which could also be contributing to the poor performance of CNF-AL<sub>5</sub>-PCL.



417  
 418 **Figure 5.** a.) Image and diagram of fast-degrading thermal sensor. b.) Total resistance change of  
 419 the thermal sensor during five cycles of heating and cooling at 20 min intervals between 15 and  
 420 50 °C. c.) Total resistance change measured when the thermal sensor was placed into contact with  
 421 a heated beaker of water at 45 °C.

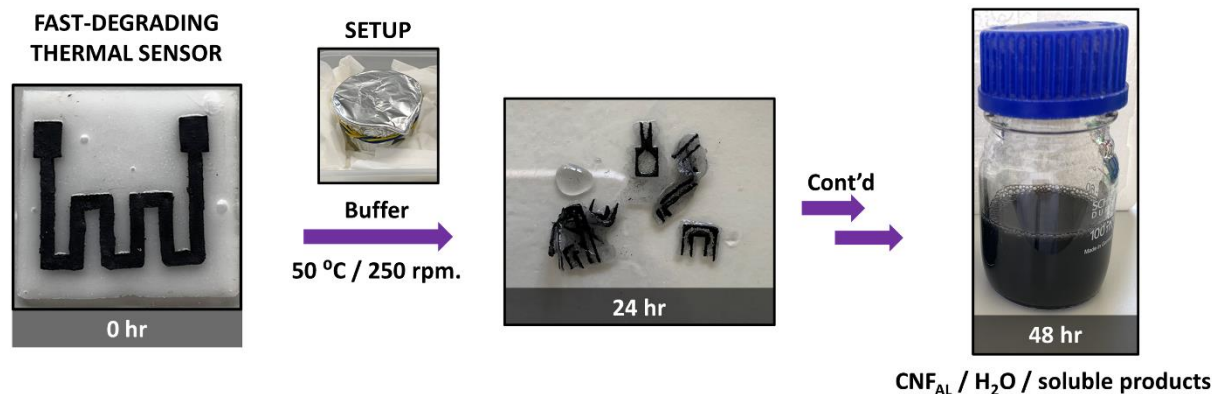
422 *Fabrication, Testing, and Degradation of Thermal Sensor*

423 To examine the applicability of these fast-degrading materials a thermal sensor was fabricated  
424 using a CNF<sub>AL</sub>-PCL electrode and an AL<sub>5</sub>-PCL support material, AL<sub>5</sub>-PCL was chosen as support  
425 as it is the fastest degrading non-conductive composite. The sensor electrodes were prepared by  
426 laser scribing pressed films of CNF<sub>AL</sub>-PCL into a serpentine pattern (Figure S8.) using a CO<sub>2</sub> laser  
427 cutting machine at room temperature. Additionally, a square support (30 mm<sup>2</sup>) made from AL<sub>5</sub>-  
428 PCL was also cut via laser scribing and fused to the CNF<sub>AL</sub>-PCL electrode via hot-pressing at 55  
429 °C to form the sensor (Figure 5a.).

430 To test the performance of the fast-degrading thermal sensor the device was placed into an  
431 environmental testing chamber (30% relative humidity (RH)) and the temperature was cycled from  
432 15 to 50 °C five times with 20 min resting intervals at each temperature while the overall resistance  
433 was monitored (Figure 5b.). From the cycling experiments the sensor was found to display a  
434 significant and repeatable electric response between 15 and 50 °C, indicating a positive  
435 temperature coefficient (PTC). Semi-crystalline thermoplastic polyesters, such as PCL, can be  
436 used as thermal sensing substrates due to the transformation of the crystalline phase to the  
437 amorphous phase as the temperature changes.<sup>38</sup> When CNF<sub>AL</sub>-PCL is heated close to its melting  
438 point (around 50 °C), the crystalline phase of PCL becomes amorphous, which results in  
439 volumetric expansion and enlarges the distance between the CNF fibers. Once the conductive  
440 composite is cooled down, the polymer begins to recrystallize, which then reforms the conductive  
441 pathways. During this experiment only a minor change in performance was observed between the  
442 first and fifth cycle with the line shape conserved throughout, however, a limited amount of  
443 baseline drift was noted. Clearly optimization is still required to increase the sensitivity and in  
444 particular stability over time of this initial proof-of-concept device. The sensor was also tested

445 outside of the environmental chamber to observe its behavior in non-ideal conditions by attaching  
446 and detaching it to a beaker of warm water at 45 °C and measuring its response (Figure 5c.). As  
447 the sensor was placed onto the warm beaker of water ( $t = \sim 17$  min), it showed an immediate  
448 response to the change in temperature reaching a maximum change in overall resistance within  $\sim 3$   
449 mins. When it was detached, it initially showed an immediate and steep drop in resistance,  
450 however, it took far longer for it to relax back to the original value. This long equilibrium time  
451 was also noted when the sensor was monitored in the environmental chamber during repeated  
452 heating and cooling cycles (Figure S9.).

453 The degradability of the thermal sensor was then tested under ideal laboratory conditions. The  
454 sensor was placed into a glass beaker, suspended in buffer, covered, and placed into an orbital  
455 incubator shaker at 50 °C and RCF = 1.05 x g (Figure 6.). This temperature was chosen as it is  
456 listed as the optimum temperature for AL from the manufacturer, however, the enzyme is active  
457 at a wide range of temperatures and has been shown to degrade PCL while embedded even at 37  
458 °C.<sup>15</sup> After 24 hours the AL<sub>5</sub>-PCL support had completely degraded with only small pieces of the  
459 CNF<sub>AL</sub>-PCL electrode left over. The remnants of the electrode were then allowed to react in the  
460 same buffer solution for an additional 24 hours (total 48 hours) where it fully degraded only leaving  
461 finely suspended CNF<sub>AL</sub> and soluble organic degradation products (Figure 6.) as evidenced by  
462 centrifugation of the resultant solution.



463  
 464 **Figure 6.** Images of the fast-degrading thermal sensor over a 48-hour degradation period. The  
 465 films are placed in a beaker, filled with buffer, covered, and placed in an incubator shaker at 50 °C  
 466 and RCF = 1.05 x g (setup). After 48 hours no film is observed and only CNF, water, and soluble  
 467 degradation products remain after centrifugation.

468  
 469 SUMMARY AND CONCLUSIONS

470 Here we report the development of a fast-degrading conductive thermoplastic made from  
 471 environmentally benign materials and the fabrication of a thermal sensor from this thermoplastic  
 472 that rapidly degrades in the presence of warm water. To produce this material, we have shown that  
 473 AL can be successfully immobilized onto carbon nanofibers and compounded with PCL, retaining  
 474 its activity, to produce the fast-degrading material CNF<sub>AL</sub>-PCL. During degradation trials it was  
 475 demonstrated that CNF<sub>AL</sub>-PCL greatly outperformed the positive control CNF-AL<sub>5</sub>-PCL where  
 476 AL was not immobilized onto CNF. This difference in performance was attributed to the fact that  
 477 CNF<sub>AL</sub>-PCL has more channels on the surface of the film, and it fractures more easily during the  
 478 degradation process allowing for more water to penetrate the polymer matrix and activate the  
 479 immobilized lipase. It was also demonstrated that CNF<sub>AL</sub>-PCL can be fabricated into an electrode  
 480 and integrated with other components to produce a proof-of-concept thermal sensor that can be

481 degraded completely in 48 hours in the presence of warm water. Although more work is needed to  
482 further optimize these types of devices and reduce the long relaxation times, the material  
483 CNF<sub>AL</sub>-PCL is believed to be a promising environmentally benign solution for green electronics  
484 applications in the future.

485

486 ASSOCIATED CONTENT

#### 487 **Supporting Information.**

488 Supporting Information includes additional experimental methods, CNF characterization, SEM  
489 images of composites, composite weight percent information, electrical performance, LCMS, and  
490 sensor testing.

491 AUTHOR INFORMATION

#### 492 **Corresponding Author**

493 Angelique F. Greene, PhD. — Scion, Te Papa Tipu Innovation Park, 49 Sala Street, Rotorua 3010,  
494 New Zealand; Phone: +64 7 343 5864; [angelique.greene@scionresearch.com](mailto:angelique.greene@scionresearch.com)

#### 495 **Author Contributions**

496 AFG<sup>‡</sup> and RA<sup>‡</sup> contributed equally to the conceptualization of the idea, design of primary  
497 experiments, and authorship of this publication. AV contributed to the idea and design of key  
498 experiments. YC, QT, and BT performed experiments related to degradation of plastics and SEM,  
499 and sensor fabrication. RR and MB contributed thermomechanical analysis of polymers, MP and  
500 EG contributed to the molecular weight analysis of degraded samples, and TS contributed to  
501 fluorescence microscopy experiments. KP & MW contributed to key evaluation of results.

502 **Funding Sources**

503 This work was funded by the New Zealand Ministry of Business, Innovation and Employment  
504 (MBIE) in the framework of the Strategic Science Investment Fund.

505 **ABBREVIATIONS**

506 **PBA**, 1-pyrenebutyric acid; **AL**, Amano Lipase; **CNF**, carbon nanofiber; **CNF<sub>PBA</sub>**, carbon  
507 nanofiber functionalized with PBA; **CNF<sub>AL</sub>**, carbon nanofiber functionalized with Amano lipase;  
508 **PCL**, polycaprolactone; **CNF-PCL**, composite made from PCL and CNF; **CNF<sub>AL</sub>-PCL**,  
509 composite made from CNF<sub>AL</sub> and PCL; **CNF-AL<sub>5</sub>-PCL**, composite made from CNF, AL (5wt.%),  
510 and PCL; **AL<sub>1</sub>-PCL**, composite made from AL (1wt.%) and PCL; **AL<sub>5</sub>-PCL**, composite made  
511 from AL (5 wt.%) and PCL.

512

513 **REFERENCES**

- 514 (1) Knott, B. C.; Erickson, E.; Allen, M. D.; Gado, J. E.; Graham, R.; Kearns, F. L.; Pardo, I.;  
515 Topuzlu, E.; Anderson, J. J.; Austin, H. P.; Dominick, G.; Johnson, C. W.; Rorrer, N. A.;  
516 Szostkiewicz, C. J.; Coperić, V.; Payne, C. M.; Woodcock, H. L.; Donohoe, B. S.; Beckham, G.  
517 T.; McGeehan, J. E. Characterization and Engineering of a Two-Enzyme System for Plastics  
518 Depolymerization. *Proc. Natl. Acad. Sci.* **2020**, *117* (41), 25476–25485.  
519 <https://doi.org/10.1073/pnas.2006753117>.
- 520 (2) Lu, H.; Diaz, D. J.; Czarnecki, N. J.; Zhu, C.; Kim, W.; Shroff, R.; Acosta, D. J.; Alexander,  
521 B. R.; Cole, H. O.; Zhang, Y.; Lynd, N. A.; Ellington, A. D.; Alper, H. S. Machine Learning-  
522 Aided Engineering of Hydrolases for PET Depolymerization. *Nature* **2022**, *604* (7907), 662–  
523 667. <https://doi.org/10.1038/s41586-022-04599-z>.

- 524 (3) Son, H. F.; Cho, I. J.; Joo, S.; Seo, H.; Sagong, H.-Y.; Choi, S. Y.; Lee, S. Y.; Kim, K.-J.  
525 Rational Protein Engineering of Thermo-Stable PETase from *Ideonella Sakaiensis* for Highly  
526 Efficient PET Degradation. *ACS Catal.* **2019**, *9* (4), 3519–3526.  
527 <https://doi.org/10.1021/acscatal.9b00568>.
- 528 (4) Carrington, D.; editor, D. C. E. New Super-Enzyme Eats Plastic Bottles Six Times Faster. *The*  
529 *Guardian*. September 28, 2020. [https://www.theguardian.com/environment/2020/sep/28/new-](https://www.theguardian.com/environment/2020/sep/28/new-super-enzyme-eats-plastic-bottles-six-times-faster)  
530 [super-enzyme-eats-plastic-bottles-six-times-faster](https://www.theguardian.com/environment/2020/sep/28/new-super-enzyme-eats-plastic-bottles-six-times-faster) (accessed 2023-03-20).
- 531 (5) *Can plastic-eating enzymes solve the recycling problem?*  
532 <https://channels.ft.com/en/rethink/can-plastic-eating-enzymes-solve-the-recycling-problem/>  
533 (accessed 2023-03-20).
- 534 (6) *This AI-Designed Enzyme Can Devour Plastic Trash In Hours: Video.*  
535 [https://www.forbes.com/sites/davidrvetter/2022/04/28/scientists-use-ai-to-make-an-enzyme-](https://www.forbes.com/sites/davidrvetter/2022/04/28/scientists-use-ai-to-make-an-enzyme-that-eats-plastic-trash-in-hours-video/?sh=378e3466da6b)  
536 [that-eats-plastic-trash-in-hours-video/?sh=378e3466da6b](https://www.forbes.com/sites/davidrvetter/2022/04/28/scientists-use-ai-to-make-an-enzyme-that-eats-plastic-trash-in-hours-video/?sh=378e3466da6b) (accessed 2023-03-20).
- 537 (7) *An engineered PET depolymerase to break down and recycle plastic bottles | Nature.*  
538 <https://www.nature.com/articles/s41586-020-2149-4> (accessed 2023-03-20).
- 539 (8) Kortsha, M. *Plastic-eating Enzyme Could Eliminate Billions of Tons of Landfill Waste.* UT  
540 News. [https://news.utexas.edu/2022/04/27/plastic-eating-enzyme-could-eliminate-billions-](https://news.utexas.edu/2022/04/27/plastic-eating-enzyme-could-eliminate-billions-of-tons-of-landfill-waste/)  
541 [of-tons-of-landfill-waste/](https://news.utexas.edu/2022/04/27/plastic-eating-enzyme-could-eliminate-billions-of-tons-of-landfill-waste/) (accessed 2023-03-20).
- 542 (9) Leitão, A. L.; Enguita, F. J. Structural Insights into Carboxylic Polyester-Degrading Enzymes  
543 and Their Functional Depolymerizing Neighbors. *Int. J. Mol. Sci.* **2021**, *22* (5), 2332.  
544 <https://doi.org/10.3390/ijms22052332>.
- 545 (10) Rosato, A.; Romano, A.; Totaro, G.; Celli, A.; Fava, F.; Zanaroli, G.; Sisti, L. Enzymatic  
546 Degradation of the Most Common Aliphatic Bio-Polyesters and Evaluation of the Mechanisms

- 547 Involved: An Extended Study. *Polymers* **2022**, *14* (9), 1850.  
548 <https://doi.org/10.3390/polym14091850>.
- 549 (11) Sayyed, R. Z.; Wani, S. J.; Alyousef, A. A.; Alqasim, A.; Syed, A.; El-Enshasy, H. A.  
550 Purification and Kinetics of the PHB Depolymerase of Microbacterium Paraoxydans RZS6  
551 Isolated from a Dumping Yard. *PLOS ONE* **2019**, *14* (6), e0212324.  
552 <https://doi.org/10.1371/journal.pone.0212324>.
- 553 (12) Schwaminger, S. P.; Fehn, S.; Steegmüller, T.; Rauwolf, S.; Löwe, H.; Pflüger-Grau, K.;  
554 Berensmeier, S. Immobilization of PETase Enzymes on Magnetic Iron Oxide Nanoparticles  
555 for the Decomposition of Microplastic PET. *Nanoscale Adv.* **2021**, *3* (15), 4395–4399.  
556 <https://doi.org/10.1039/D1NA00243K>.
- 557 (13) Hegyesi, N.; Zhang, Y.; Kohári, A.; Polyák, P.; Sui, X.; Pukánszky, B. Enzymatic  
558 Degradation of PLA/Cellulose Nanocrystal Composites. *Ind. Crops Prod.* **2019**, *141*, 111799.  
559 <https://doi.org/10.1016/j.indcrop.2019.111799>.
- 560 (14) Ganesh, M.; Dave, R. N.; L'Amoreaux, W.; Gross, R. A. Embedded Enzymatic  
561 Biomaterial Degradation. *Macromolecules* **2009**, *42* (18), 6836–6839.  
562 <https://doi.org/10.1021/ma901481h>.
- 563 (15) Greene, A. F.; Vaidya, A.; Collet, C.; Wade, K. R.; Patel, M.; Gaugler, M.; West, M.;  
564 Petcu, M.; Parker, K. 3D-Printed Enzyme-Embedded Plastics. *Biomacromolecules* **2021**, *22*  
565 (5), 1999–2009. <https://doi.org/10.1021/acs.biomac.1c00105>.
- 566 (16) DelRe, C.; Jiang, Y.; Kang, P.; Kwon, J.; Hall, A.; Jayapurna, I.; Ruan, Z.; Ma, L.; Zolkin,  
567 K.; Li, T.; Scown, C. D.; Ritchie, R. O.; Russell, T. P.; Xu, T. Near-Complete  
568 Depolymerization of Polyesters with Nano-Dispersed Enzymes. *Nature* **2021**, *592* (7855),  
569 558–563. <https://doi.org/10.1038/s41586-021-03408-3>.

- 570 (17) Huang, Q.; Hiyama, M.; Kabe, T.; Kimura, S.; Iwata, T. Enzymatic Self-Biodegradation  
571 of Poly(l-Lactic Acid) Films by Embedded Heat-Treated and Immobilized Proteinase K.  
572 *Biomacromolecules* **2020**, *21* (8), 3301–3307. <https://doi.org/10.1021/acs.biomac.0c00759>.
- 573 (18) Thoden van Velzen, E. U.; Santomasi, G. Tailor-Made Enzymes Poised to Propel Plastic  
574 Recycling into a New Era. *Nature* **2022**, *604* (7907), 631–633.  
575 <https://doi.org/10.1038/d41586-022-01075-6>.
- 576 (19) *New process makes 'biodegradable' plastics truly compostable | College of Chemistry.*  
577 <https://chemistry.berkeley.edu/news/new-process-makes->  
578 [%E2%80%98biodegradable%E2%80%99-plastics-truly-compostable-0](https://chemistry.berkeley.edu/news/new-process-makes-%E2%80%98biodegradable%E2%80%99-plastics-truly-compostable-0) (accessed 2023-03-  
579 21).
- 580 (20) *Compostables-Packaging-Position-Statement.Pdf.*  
581 [https://environment.govt.nz/assets/publications/compostables-packaging-position-](https://environment.govt.nz/assets/publications/compostables-packaging-position-statement.pdf)  
582 [statement.pdf](https://environment.govt.nz/assets/publications/compostables-packaging-position-statement.pdf) (accessed 2023-03-21).
- 583 (21) Suciu, G.; Ciuciuc, R.; Pasat, A.; Scheianu, A. Remote Sensing for Forest Environment  
584 Preservation. In *Recent Advances in Information Systems and Technologies*; Rocha, Á.,  
585 Correia, A. M., Adeli, H., Reis, L. P., Costanzo, S., Eds.; Advances in Intelligent Systems and  
586 Computing; Springer International Publishing: Cham, 2017; pp 211–220.  
587 [https://doi.org/10.1007/978-3-319-56538-5\\_23](https://doi.org/10.1007/978-3-319-56538-5_23).
- 588 (22) Torresan, C.; Benito Garzón, M.; O'Grady, M.; Robson, T. M.; Picchi, G.; Panzacchi, P.;  
589 Tomelleri, E.; Smith, M.; Marshall, J.; Wingate, L.; Tognetti, R.; Rustad, L. E.; Kneeshaw, D.  
590 A New Generation of Sensors and Monitoring Tools to Support Climate-Smart Forestry  
591 Practices. *Can. J. For. Res.* **2021**, *51* (12), 1751–1765. <https://doi.org/10.1139/cjfr-2020-0295>.

- 592 (23) Wiesemüller, F.; Miriyev, A.; Kovac, M. Zero-Footprint Eco-Robotics: A New Perspective  
593 on Biodegradable Robots. In *2021 Aerial Robotic Systems Physically Interacting with the*  
594 *Environment (AIRPHARO)*; 2021; pp 1–6.  
595 <https://doi.org/10.1109/AIRPHARO52252.2021.9571067>.
- 596 (24) Li, W.; Liu, Q.; Zhang, Y.; Li, C.; He, Z.; Choy, W. C. H.; Low, P. J.; Sonar, P.; Kyaw, A.  
597 K. K. Biodegradable Materials and Green Processing for Green Electronics. *Adv. Mater.* **2020**,  
598 *32* (33), 2001591. <https://doi.org/10.1002/adma.202001591>.
- 599 (25) Zhu, H.; Luo, W.; Ciesielski, P. N.; Fang, Z.; Zhu, J. Y.; Henriksson, G.; Himmel, M. E.;  
600 Hu, L. Wood-Derived Materials for Green Electronics, Biological Devices, and Energy  
601 Applications. *Chem. Rev.* **2016**, *116* (16), 9305–9374.  
602 <https://doi.org/10.1021/acs.chemrev.6b00225>.
- 603 (26) Piro, B.; Tran, H. V.; Thu, V. T. Sensors Made of Natural Renewable Materials: Efficiency,  
604 Recyclability or Biodegradability—The Green Electronics. *Sensors* **2020**, *20* (20), 5898.  
605 <https://doi.org/10.3390/s20205898>.
- 606 (27) Abbel, R.; Greene, A. F.; Quilter, H.; Leveneur, J.; Risani, R.; Barbier, M.; West, M.;  
607 Collet, C.; Kirby, N. M.; Sorieul, M. Crystallization Behavior and Sensing Properties of Bio-  
608 Based Conductive Composite Materials. *Adv. Eng. Mater.* **2023**, *25* (2), 2200959.  
609 <https://doi.org/10.1002/adem.202200959>.
- 610 (28) Beniwal, A.; Ganguly, P.; Aliyana, A. K.; Khandelwal, G.; Dahiya, R. Screen-Printed  
611 Graphene-Carbon Ink Based Disposable Humidity Sensor with Wireless Communication.  
612 *Sens. Actuators B Chem.* **2023**, *374*, 132731. <https://doi.org/10.1016/j.snb.2022.132731>.

- 613 (29) Tu, T.; Liang, B.; Cao, Q.; Fang, L.; Zhu, Q.; Cai, Y.; Ye, X. Fully Transient  
614 Electrochemical Testing Strips for Eco-Friendly Point of Care Testing. *RSC Adv.* **2020**, *10*  
615 (12), 7241–7250. <https://doi.org/10.1039/C9RA09847J>.
- 616 (30) *Challenges and opportunities of biodegradable plastics: A mini review - Maja Rujnić-*  
617 *Sokele, Ana Pilipović, 2017.*  
618 <https://journals.sagepub.com/doi/abs/10.1177/0734242X16683272?journalCode=wmra>  
619 (accessed 2023-03-21).
- 620 (31) Iwata, T. Biodegradable and Bio-Based Polymers: Future Prospects of Eco-Friendly  
621 Plastics. *Angew. Chem. Int. Ed.* **2015**, *54* (11), 3210–3215.  
622 <https://doi.org/10.1002/anie.201410770>.
- 623 (32) Kwon, J.; DelRe, C.; Kang, P.; Hall, A.; Arnold, D.; Jayapurna, I.; Ma, L.; Michalek, M.;  
624 Ritchie, R. O.; Xu, T. Conductive Ink with Circular Life Cycle for Printed Electronics. *Adv.*  
625 *Mater.* **2022**, *34* (30), 2202177. <https://doi.org/10.1002/adma.202202177>.
- 626 (33) Bozó, É.; Ervasti, H.; Halonen, N.; Shokouh, S. H. H.; Tolvanen, J.; Pitkänen, O.; Järvinen,  
627 T.; Pálvölgyi, P. S.; Szamosvölgyi, Á.; Sági, A.; Konya, Z.; Zacccone, M.; Montalbano, L.; De  
628 Brauwer, L.; Nair, R.; Martínez-Nogués, V.; San Vicente Laurent, L.; Dietrich, T.; Fernández  
629 de Castro, L.; Kordas, K. Bioplastics and Carbon-Based Sustainable Materials, Components,  
630 and Devices: Toward Green Electronics. *ACS Appl. Mater. Interfaces* **2021**, *13* (41), 49301–  
631 49312. <https://doi.org/10.1021/acsami.1c13787>.
- 632 (34) *Phosphate Buffer (pH 5.8 to 7.4) Preparation and Recipe | AAT Bioquest.*  
633 [https://www.aatbio.com/resources/buffer-preparations-and-recipes/phosphate-buffer-ph-5-8-](https://www.aatbio.com/resources/buffer-preparations-and-recipes/phosphate-buffer-ph-5-8-to-7-4)  
634 [to-7-4](https://www.aatbio.com/resources/buffer-preparations-and-recipes/phosphate-buffer-ph-5-8-to-7-4) (accessed 2023-03-21).

635 (35) Min, K.; Kim, J.; Park, K.; Yoo, Y. J. Enzyme Immobilization on Carbon Nanomaterials:  
636 Loading Density Investigation and Zeta Potential Analysis. *J. Mol. Catal. B Enzym.* **2012**, *83*,  
637 87–93. <https://doi.org/10.1016/j.molcatb.2012.07.009>.

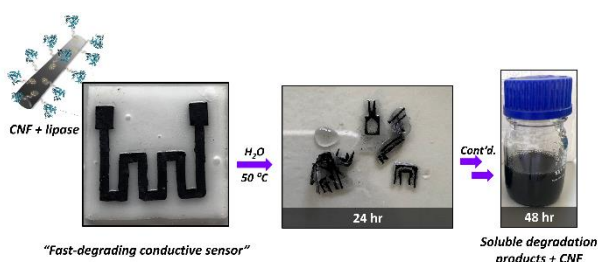
638 (36) Chang, S. K. C.; Zhang, Y. Protein Analysis. In *Food Analysis*; Nielsen, S. S., Ed.; Food  
639 Science Text Series; Springer International Publishing: Cham, 2017; pp 315–331.  
640 [https://doi.org/10.1007/978-3-319-45776-5\\_18](https://doi.org/10.1007/978-3-319-45776-5_18).

641 (37) Baptista, C.; Azagury, A.; Shin, H.; Baker, C. M.; Ly, E.; Lee, R.; Mathiowitz, E. The Effect  
642 of Temperature and Pressure on Polycaprolactone Morphology. *Polymer* 2020, *191*, 122227.  
643 <https://doi.org/10.1016/j.polymer.2020.122227>.

644 (38) Skoglund, P.; Fransson, Å. Continuous Cooling and Isothermal Crystallization of  
645 Polycaprolactone. *J. Appl. Polym. Sci.* **1996**, *61* (13), 2455–2465.  
646 [https://doi.org/10.1002/\(SICI\)1097-4628\(19960926\)61:13<2455::AID-APP25>3.0.CO;2-1](https://doi.org/10.1002/(SICI)1097-4628(19960926)61:13<2455::AID-APP25>3.0.CO;2-1).

647

648 (TABLE OF CONTENTS GRAPHIC (TOC))



649